Fluidic oscillator with active phase control

Chris J. Nicholls* and Marko Bacic†
University of Oxford, Oxford, OX2 0ES, United Kingdom

This paper demonstrates the closed-loop control of the frequency and phase of a fluidic oscillator using acoustic excitation. It is shown experimentally that the use of acoustic excitation modifies the passive feedback mechanism and slows down the jet switching process. Closed-loop control is employed to vary the oscillation frequency at a fixed flow rate and track a sinusoidal reference target without phase error, using measurements from a pitot probe in the device. The controller is demonstrated to be effective at rejecting disturbances, which is illustrated with both time and frequency domain data. The controller's ability to track step changes to the reference signal phase is tested and the closed-loop bandwidth is shown to be around 20% of the oscillation frequency, in close agreement with the theoretical prediction.

I. Nomenclature

Latin

A	=	amplitude of time-varying component of modulating signal
B	=	amplitude of carrier component of AM signal
b	=	inlet nozzle width
d	=	device depth
$D(t)$	=	oscillation signal magnitude
D_{CP}	=	control port tube diameter
D_{O}	=	outlet tube diameter
Δf	=	integration limit parameter
$f(x)$	=	gain for nonlinearity compensation
f_{c}	=	carrier frequency
f_{LPF}	=	low-pass filter cut-off frequency
f_{m}	=	modulating frequency
f_{osc}	=	oscillation frequency
$f_{\mathrm{osc,exc}}$	=	steady component of excited oscillation frequency
$f_{\mathrm{osc,nat}}$	=	unexcited oscillation frequency
f_{ref}	=	reference signal frequency
$G(s)$	=	plant transfer function
$\hat{G}(s)$	=	estimated plant transfer function
$g_{\mathrm{c}}(t)$	=	carrier component of AM signal
$g_{\mathrm{ex}}(t)$	=	AM signal applied to piezo amplifier
$g_{\mathrm{m}}(t)$	=	modulating component of AM signal
$H(x)$	=	saturation limits function
$H_{\mathrm{LPF}}(s)$	=	low-pass filter transfer function
k_{f}	=	modulation depth
K_{I}	=	integral gain
K_{p}	=	proportional gain
$L(s)$	=	open-loop transfer function
L_{CP}	=	control port tube length
L_{O}	=	outlet tube length
M	=	integrated oscillation magnitude

*Post-Doctoral Research Assistant, Oxford Thermofluids Institute, christopher.nicholls@eng.ox.ac.uk. Member AIAA.
†University Research Lecturer, Oxford Thermofluids Institute. Member AIAA. Seconded part-time to OTI from Rolls-Royce plc.

$p_{\text{out}}(t)$ = outlet channel pitot probe signal
$u(t)$ = control input, amplitude of tone applied to piezo amplifier
$u'(t)$ = PI controller output
$T(s)$ = closed-loop transfer function
$U(i\omega)$ = discrete Fourier transform of input
$y(t)$ = plant output
$Y(i\omega)$ = discrete Fourier transform of output
$Y_{\text{mix}}(s)$ = Laplace transform of mixer output
z = frequency discriminator output
$z_{f_{\text{m}}}$ = component of z at f_{m}

Greek

ϕ = phase offset of demodulated pitot signal
$\phi_{\text{e}}(t)$ = controller phase error
$\phi_{\text{r}}(t)$ = reference signal phase
$\Phi_{uu}(i\omega)$ = power spectral density of input
$\phi_{\text{y}}(t)$ = output signal phase
$\Phi_{yu}(i\omega)$ = cross spectral density of output and input

Abbreviations

AM = amplitude modulation
ETFE = empirical transfer function estimate
FM = frequency modulation
PI = proportional-integral
PLL = phase-locked loop
PSD = power spectral density
VCO = voltage-controlled oscillator

II. Introduction

This paper demonstrates for the first time the closed-loop frequency and phase control of an otherwise passive fluidic oscillator that can be used in a variety of applications where time-accurate fluid injection is required (e.g. [1, 2]). Fluidic oscillators and other fluidic devices such as fluidic diverters (see Fig. 1) originate from work at the Harry Diamond Laboratories in the 1960s for fluidic computing applications. The popularity of fluidic devices in a modern research context is a result of their potential to provide a reliable means of actuating fluid flows since they contain no moving parts [3]. Many articles have been written about their application to problems such as flow separation control [4–8], cavity tone supression [9], tip leakage control [10–12], and thrust vectoring [13]. The present work is motivated by the challenge of controlling fluid flows in aerospace applications, which typically require reliable actuators with significant authority and relatively high bandwidth [14]. Fluidic actuators have the potential to overcome these challenges, particularly when combined with piezoelectric actuators [15–18], but suffer from switching time uncertainty. More recently, Nicholls and Bacic [19] demonstrated that the use of feedback control can reduce switching time uncertainty at the expense of closed-loop bandwidth for piezo-actuated fluidic diverters. The hypothesis proven in this paper is that active sound injection can modify the passive feedback mechanism in a fluidic oscillator to create a high bandwidth, frequency- and phase-controlled actuator.

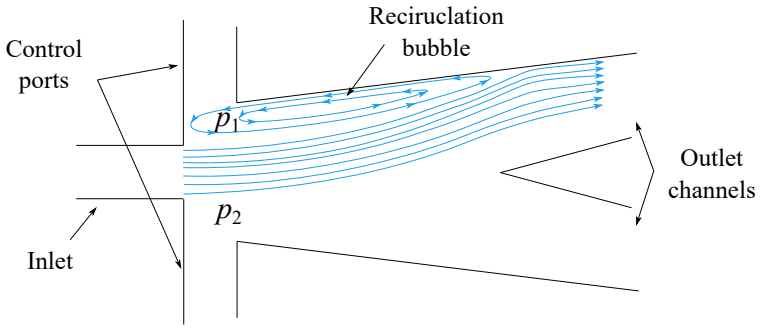

Fig. 1 Fluidic diverter

Feedback fluidic oscillators are fluidic diverters with some kind of passive feedback mechanism, allowing the device to produce self-sustained oscillations when supplied with a pressurised fluid. These typically have a higher continuous switching bandwidth than diverters that are controlled actively with either an external fluid supply or a separate actuator, e.g. plasma or acoustic. However, the oscillation frequency depends on the flow rate [20]. There are two common designs of feedback oscillators: relaxation fluidic oscillators, introduced by Warren [21] (Fig. 2b), which have two feedback paths and use a portion of the main jet total pressure to switch the flow, and 'sonic' oscillators, introduced by Spyropoulos [22] (Fig. 2a). The latter have one feedback path and use the pressure difference that keeps the jet curved and attached to the wall to drive the oscillation. The widely-used NASA relaxation fluidic oscillator design has dominated flow control studies in the literature, e.g. [1, 23, 24], with the design style by Spyropoulos [22] seeing relatively little research interest. However, the relaxation oscillator design is likely to suffer from inherently higher pressure losses because of the nature of the oscillation mechanism—momentum is bled from the main jet into the feedback paths. The sonic oscillator does not siphon off any of the main jet total pressure, which could make it appealing in industrial applications.

Practical fluidic devices are governed by the Coandă effect, the tendency of a fluid jet to attach to a nearby surface [25]. When supplied with a pressurised fluid, a jet issues from a nozzle and entrains the surrounding ambient fluid (Fig. 1). The jet surroundings are confined by the attachment walls, which causes the pressure on either side to reduce. Geometrical imperfections or random perturbations result in an asymmetry in the pressure reduction, resulting in the jet attaching to one of the side walls. Upon striking the wall, the angle of the jet and the low pressure between the jet and the wall cause flow to be recirculated into the enclosed region. This stabilises the pressure there and a recirculation bubble is formed.

Spyropoulos [22] proposed a fluidic oscillator design where feedback is provided by a tube connecting the sides of the

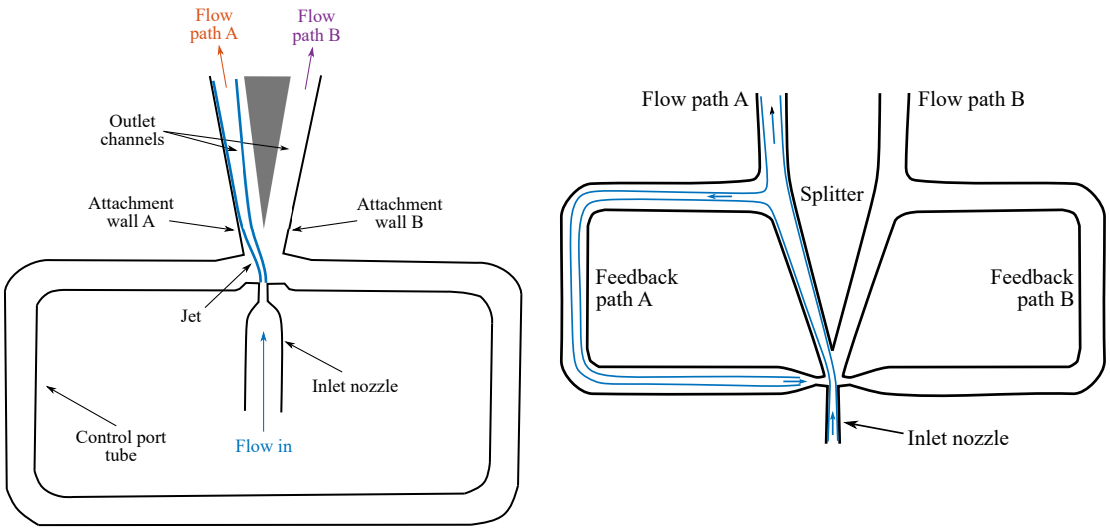

(a) Sonic oscillator, proposed by Spyropoulos [22].

(b) Relaxation fluidic oscillator, proposed by Warren [21].

Fig. 2 Sonic oscillator, 2a, and relaxation fluidic oscillator, 2b.

device to one another (Fig. 2a). When the jet attaches to wall A, the sharp pressure reduction between the jet and the wall creates an expansion wave that travels along the control port tube (to B in Fig. 2a). The wave connects the sides of the jet, but is typically insufficient to switch the device alone because it is attenuated as it travels around the tube. The remaining pressure deficit is relieved by fluid supplied from the unattached side outlet (reversed flow through Flow path B) via the control port tube to side A, causing the jet to switch to wall B, where the process repeats. The jet oscillates between paths A and B.

Both types of feedback fluidic oscillator are 'passively-controlled' because their operation requires no switching input, and they provide large-amplitude, high-frequency oscillations. The absence of control over the phase, however, reduces their versatility in timing-critical applications. For example, it has been shown that synchronization of unsteady injection from an aerofoil into the mainstream flow improves the effectiveness of the actuation in reattaching separated flows [1, 2]. Efforts have been made to address this drawback by the addition of an active control element to the NASA relaxation oscillator design. In a numerical study, Gokoglu et al. [24] demonstrated that plasma actuators placed in the feedback paths should have sufficient authority to disrupt the feedback mechanism and bring the oscillation frequency under control. More recently, Tomac and Sundström [26] brought the oscillation frequency of a relaxation oscillator under control by the injection of secondary flows into the interaction region. With a sufficient control flow rate, it was shown that the flow instabilities generated from the interaction between the control and main jets dominated the traditional feedback mechanism and resulted in significantly higher oscillation frequencies. These studies have made good progress towards bringing the oscillation signal under control. However, one drawback of using secondary flows in [26], as mentioned by the authors, is the requirement to modulate the control flow rate in order to regulate the oscillation

frequency. A second downside is the lack of control over the oscillation phase. This latter point was solved in part by Sundström and Tomac [23, 27], where it was shown that it is possible to synchronize the phase of a pair of oscillators by designing them to share a feedback path. However, the ideal situation would be the ability to lock the oscillation phase of an arbitrary number of spatially-distinct devices to a reference signal without the use of secondary control flows.

This paper aims to address these issues by using acoustic actuation to vary the oscillation frequency and control the phase with respect to a reference signal. We achieve this through use of an architecture based on a phase-locked loop (PLL), a technique commonly used in communications. Gharib [28] applied a PLL to the closed-loop control of a cavity shear layer. Stalnov et al. [29] used a PLL to lock trailing edge actuation to a constant phase shift with respect to the vortical structures shed from a bluff body measured by a hot film sensor in order to stabilise the wake. Previous work demonstrated that piezoelectric excitation can influence the jet position in a fluidic device [19]. In the present work, it is shown that when applied to a fluidic oscillator, piezoelectric actuation slows down the switching process and hence reduces the oscillation frequency. This effect is used in conjunction with feedback control to vary the frequency and phase of a Spyropoulos sonic oscillator.

III. Experimental setup

The experimental setup is shown in Fig. 3a, with a photograph of the rapid-prototyped device in Fig. 3b The field programmable gate array (FPGA) used is the National Instruments (NI) cRIO-9035, with the NI 9205 analog input card and NI 9263 analog output card. The flow path for the oscillator used in the present work is shown in Fig. 4. The feedback tube, called the control port (CP) tube in this paper, connects into the plane of Figures 4a and 4b to the slots shown in the control ports, as shown in Fig. 4c. The device is a sonic oscillator with a rectangular nozzle of width $b = 2$ mm and depth $d = 6$ mm, with the addition of piezo buzzers (Kingstate 108 dB Panel Mount Continuous External Piezo Buzzer). Throughout this paper, only one of the piezo buzzers is used. The excitation signals are amplified by a piezo amplifier (PiezoDrive PDu150). Outlet tubes of length $L_O = 20$ cm and internal diameter $D_O = 4b$ are fitted via an adapter to the main device outlets. The control port tube has length $L_{CP} = 40$ cm and $D_{CP} = 4b$. Pressure transducers (First Sensor 10 mbar HCXPM010D6V) connected to the pitot probes are sampled at 50 kHz. The transducers have a response time of 100 µs (i.e. 10 kHz bandwidth) and were sampled via a first order anti-aliasing filter with a cut-off frequency of 25 kHz. The transducers have a typical accuracy of 0.1% of the full scale output. Short lengths of 1.65 mm Scanivalve tubing are used to connect the pitot tappings on the device to the transducers, which lowers their measurement bandwidth. However, the length was kept sufficiently small to insure the tube bandwidth exceeded the device oscillating frequency and open-loop bandwidth. The bandwidth of the transducers with the tubes was assessed by removing the control port tube and blocking the control ports such that the jet was stably attached to one of the device. The fluctuations in the jet act as a band-limited noise input to the measurement transfer function. As such, the pitot

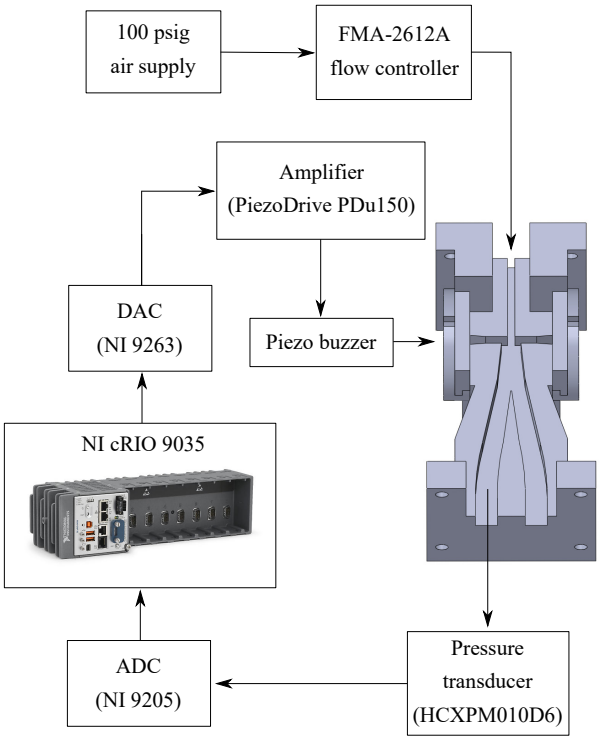

(a) Experimental setup

(b) Photograph of device manufactured by rapid prototyping

Fig. 3 Experimental setup and device photograph

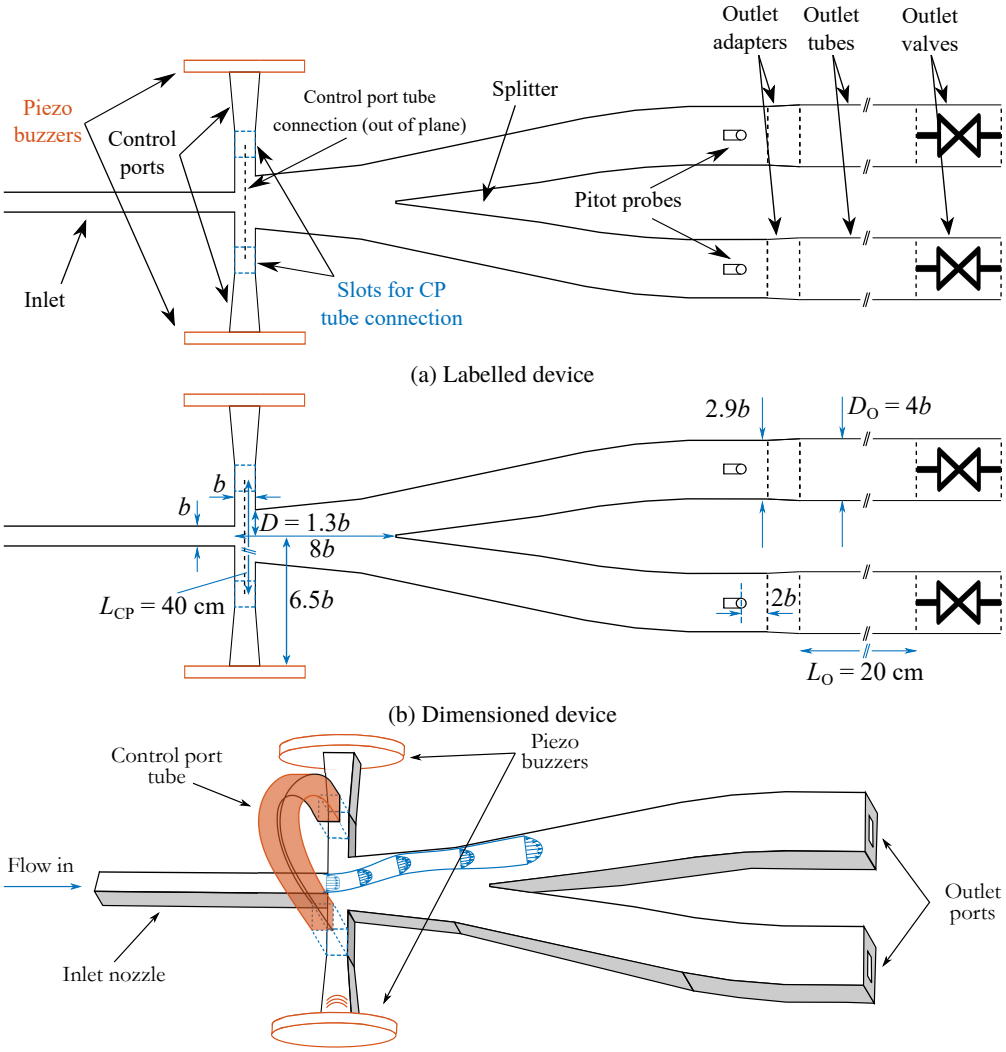

(a) Labelled device

(b) Dimensioned device

(c) 3D device flow path, not including outlet tubes or outlet valves

Fig. 4 Flow path for device in the present work

signal was measured and the power spectral density was computed, giving a measurement bandwidth of 520 Hz. The outlet ball valves are partially closed to supply a small back pressure, which serves to increase the oscillation magnitude, which is otherwise intermittent. As explained in Nicholls et al. [30], the back pressure has the effect of reducing the jet attachment strength in the quasi-steady portion of the oscillation period where the jet is stably attached to one of the walls. This is because the adverse pressure gradient experienced by the diffusing flow increases the likelihood of separation and has a destabilising effect on attachment. This makes it easier for the oscillation mechanism (the flow through the control port tube) to switch the jet. In this paper, the device operates in the traditional, flow-rate dependent mode characterised by Spyropoulos [22], rather than the back-pressure driven mode described by Nicholls et al. [30].

IV. Device characterisation

The device was characterised with respect to flow rate with and without excitation from the piezo buzzer. The excitation was a 0.71 V_{RMS}, 2.5 kHz tone. At this frequency and voltage, the piezo produces a sound pressure level of approximately 111 dB when measured at a distance of 13 mm (to match the distance between the piezo and the jet in the device (Fig.4b)). It should be noted that this distance is around 10% of the wavelength of the acoustic excitation signal. As such, the jet is in the near field of the buzzer and the forcing is hydrodynamic. This excitation frequency was chosen because it is the resonant frequency of the piezo buzzers. For each case, 200,000 samples were recorded over 4 seconds. The samples were split up into 4 sections and their FFTs were taken after a Hamming window was applied. The absolute value of the resulting data was taken before the 4 sections were ensemble averaged. The power spectral density (PSD) was then computed by squaring these ensemble-averaged data, which produced 25001 samples over the 25 kHz bandwidth, giving a frequency resolution of 1 Hz. Note that this process is identical to Bartlett's method [31] (i.e. Welch's method with 0 overlap [32]) except that, in our case, the averaging step is performed before the discrete Fourier transform data are squared. The difference in the resulting PSD estimate between this approach and Bartlett's method is negligible. The oscillation frequency, f_{osc}, was determined at each flow rate from the spectrum of the pitot probe measurements. These data and their difference, Δf_{osc}, are shown in Fig. 5. The unexcited curve is typical of a sonic oscillator and in agreement with previous studies [22, 30, 33]. The effect of excitation is to lower the oscillation frequency for all but the lowest flow rates. The device did not oscillate for flow rates below 20 slpm, and the piezo authority gradually reduced from its maximum at around 60 slpm until 140 slpm where its effect was not noticeable. The acoustic excitation has a significant impact on the oscillation frequency at some flow rates; at 55 slpm, the frequency is reduced by 15%.

The components of the oscillation period are the wave propagation time and the switching time [22]. The switching time can be further divided into the time taken for the recirculation bubble (see Fig. 1) to be filled to reach the critical volume where the jet detaches (herein called the filling time), and the time taken for the jet to travel across the device and reattach to the opposite wall. This division is consistent with the models of fluidic devices actuated with control flows by Lush

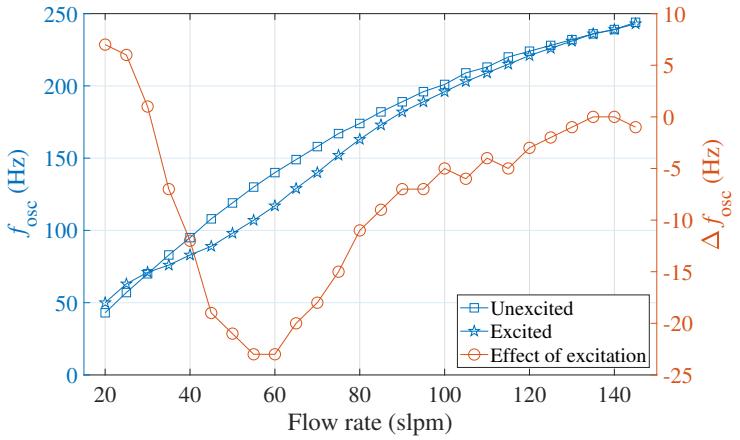

Fig. 5 Oscillation frequency vs flow rate: Unexcited (blue, squares), and excited with 0.71 V_{rms}, 2.5 kHz tone (blue, stars); difference between excited and unexcited oscillation frequencies (red, circles).

[34, 35] and Epstein [36]. Understanding the mechanism by which the acoustic excitation influences the oscillation period requires more sophisticated measurement techniques or numerical simulations. However, the proposed mechanism is that the enhanced entrainment resulting from the excitation [37] removes mass from the bubble at a greater rate, so that it takes longer for the flow through the control port tube to fill the bubble and reach the critical volume required for switching.

The second effect of excitation is a reduction in the amplitude of the oscillation. The oscillation magnitude and frequency were determined from the spectra of the measurements at a range of excitation voltages and are shown in Fig. 6 for 60–70 slpm. The magnitudes were determined by integrating the power spectral density (PSD) across the peak, as given by

$$M = 10 \log_{10} \left(\frac{1}{2\Delta f} \int_{f_{osc}-\Delta f}^{f_{osc}+\Delta f} S_{yy}(f)\, \mathrm{d}f \right), \tag{1}$$

with the integration limits set using $\Delta f = 5$ Hz and a 1 Pa^2 reference for the logarithm. The power is not packed into a single frequency bin because disturbances like small variations in the flow rate cause the frequency and phase to wander. The value of 5 Hz was chosen for the limit range because it captured a sufficient proportion of the spectral peak that increasing it had an insignificant effect on the resulting oscillation magnitude, M. One explanation for the reduction in oscillation magnitude is that the device can be considered a resonant system with a magnitude peak at the unexcited oscillation frequency. When the excitation modifies the feedback mechanism and reduces the frequency, the device operates away from its resonance, which reduces the oscillation magnitude. The data show a linear response in both the frequency and in the oscillation magnitude (in units of dB) to excitation—these are plotted against one another in Fig. 6c. Figure 6a demonstrates that the oscillation amplitude, in linear units rather than dB, varies nonlinearly with respect to the excitation voltage. As such, a compensation strategy is required to invert this nonlinearity for a linear control design approach to be valid.

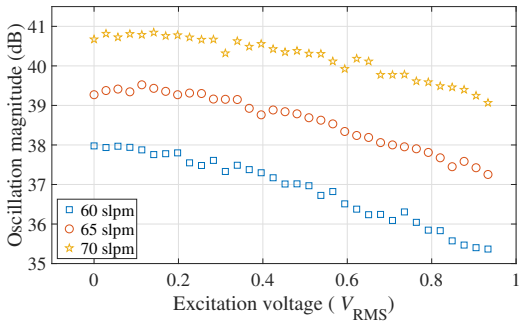

(a) Integrated oscillation magnitude (f_{osc} ± 5 Hz) vs excitation voltage at several flow rates.

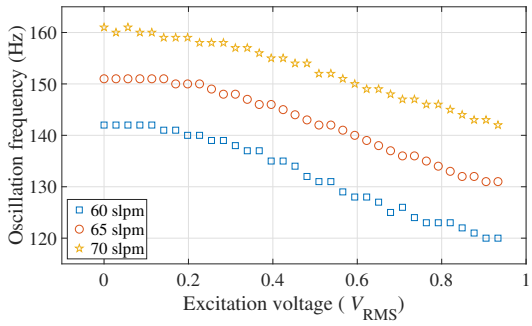

(b) Oscillation frequency vs excitation voltage at several flow rates.

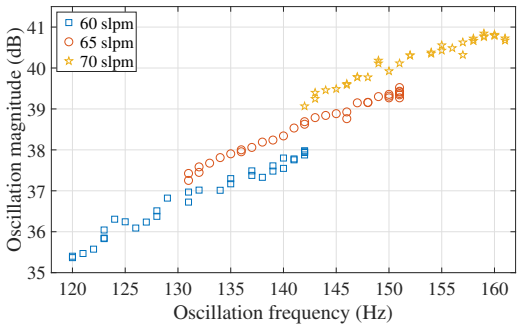

(c) Integrated oscillation magnitude (f_{osc} ± 5 Hz) vs oscillation frequency.

Fig. 6 Oscillation magnitude (6a) and frequency (6b) vs excitation voltage, and oscillation magnitude vs oscillation frequency (6c) at 60–70 slpm.

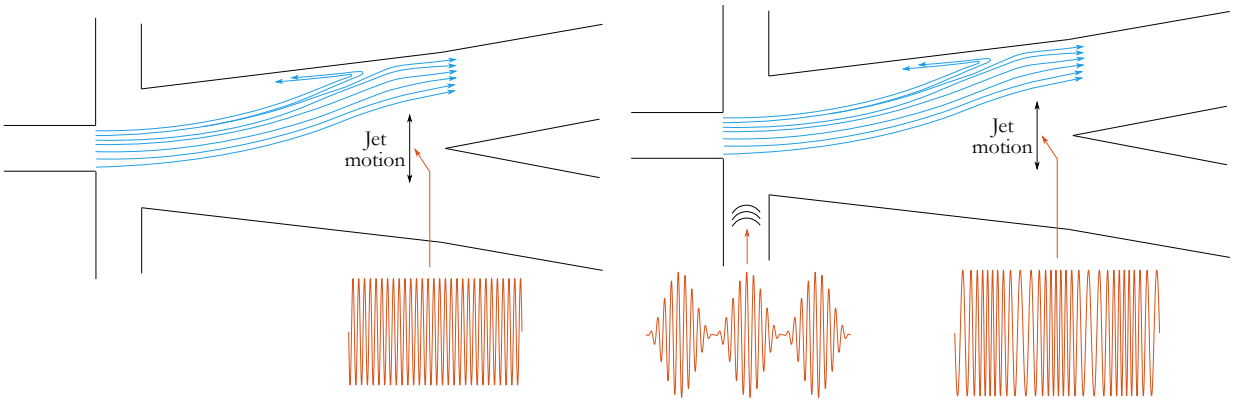

(a) No excitation

(b) AM excitation waveform

Fig. 7 Pictographic representation of AM to FM conversion in oscillator

V. System Identification

In order to vary the oscillation frequency dynamically, the amplitude of the excitation tone must be modulated. The amplitude modulation (AM) input signal is given by

$$g_{\text{ex}}(t) = g_{\text{c}}(t)g_{\text{m}}(t) = \sin\left(2\pi f_{\text{c}} t\right)\left(A\sin\left(2\pi f_{\text{m}} t\right) + B\right), \tag{2}$$

where A is the amplitude of the time-varying component of the modulation signal, B is the carrier offset amplitude, f_{c} is the carrier frequency (2.5 kHz in this paper), and f_{m} is the modulating frequency. The jet demodulates this signal, a property first discovered by Wiltse and Glezer [38]. For an attached jet without a feedback tube, as in a fluidic diverter, a constant excitation causes the jet to be pulled off the wall. Therefore, modulating the amplitude of the tone results in the jet responding at the modulating frequency, f_{m}, which has been exploited in several studies, e.g. [19, 39]. With the addition of the feedback tube, this demodulated signal is then modulated onto the oscillating frequency of the device. This process is represented graphically in Fig. 7. Figure 7a shows the unexcited case, where the jet motion (switching between the two sides) is portrayed as a single sinusoid. An AM excitation waveform is applied in Fig. 7b, and the frequency of the jet oscillation is shown to fluctuate with the envelope of the excitation waveform. The resulting frequency modulation (FM) signal in response to the AM excitation is given by

$$p_{\text{out}} = D(t)\sin\left(2\pi\left[f_{\text{osc,exc}}\, t + k_{\text{f}}\int_{\tau=0}^{\tau=t}\sin\left(2\pi f_{\text{m}}\tau + \phi\right)\,\mathrm{d}\tau\right]\right), \tag{3}$$

where k_{f} is the modulation depth, ϕ is a phase offset, and $D(t)$ is the oscillation amplitude that depends on the excitation voltage (Fig. 6a). The formula in (3) is a standard expression for an FM signal [40, p. 204], with the addition of a time-varying amplitude, $D(t)$. It is around $f_{\text{osc,exc}}$ that the oscillation frequency varies sinusoidally at a rate of f_{m}. Note that $f_{\text{osc,exc}}$ differs from the natural, unexcited value, $f_{\text{osc,nat}}$, because of the carrier component in (2) with amplitude B,

which reduces it. When a constant (not amplitude-modulated) excitation tone is switched on, the oscillation frequency does not drop to $f_{\mathrm{osc,exc}}$ instantly—the oscillation frequency is related to the cross-stream speed of the bulk jet, so that an instantaneous change in frequency would constitute an infinite acceleration. The bulk jet dynamics, as controlled by Nicholls and Bacic [19], are important in the response of the oscillation frequency to the excitation signal. This system has the transfer function

$$G(s) = \frac{\mathcal{L}\left\{f_{\mathrm{osc}}(t) - f_{\mathrm{osc,exc}}\right\}}{\mathcal{L}\left\{g_{\mathrm{m}}(t) - B\right\}}. \tag{4}$$

The value of the modulation depth in (3), k_{f}, is equal to $|G\left(i2\pi f_{\mathrm{m}}\right)|$. Similarly, the phase, ϕ, is determined by $\angle G(i2\pi f_{\mathrm{m}})$ and the system transport delay. For the purposes of system identification, the input and output are given by

$$u(t) = g_{\mathrm{m}}(t) - B, \qquad y(t) = f_{\mathrm{osc}}(t) - f_{\mathrm{osc,exc}}. \tag{5}$$

The output, $y(t)$, is therefore the time-varying component of the signal that is frequency modulated onto the oscillation signal measured by the pitot probe (i.e. the time-varying component of the frequency of the sinusoid in (3)). Experiments were conducted to determine the transfer function, $G(s)$, at several flow rates using the AM input signal, (2). For each flow rate, A and B were set to ensure the static response curve of oscillation frequency against excitation amplitude (as in Fig. 6b) remained in the linear region. A frequency discriminator was applied to the data to demodulate the measured signal and retrieve the output, (5). Details of this scheme and an analysis of its effect on the signal spectrum are given in the appendix. The oscillation amplitude, D, is present in the demodulated signal, and the analysis assumes that it is a constant. As such, the curve of oscillation magnitude vs excitation voltage in Fig. 6a was inverted for each flow rate by appropriate scaling of the inputs, $u(t)$. This inversion is discussed in more detail in section VI. The analysis in the appendix also shows that the demodulated signal phase is independent of the oscillation signal phase ($f_{\mathrm{osc,exc}}\, t$), so that phase-coherent averaging could be used to improve the signal-to-noise ratio. The excitation was applied for 4 seconds for each value of f_{m}, and 10 repeats were conducted to create an ensemble. After demodulation, followed by ensemble averaging, the empirical transfer function estimate (ETFE) was calculated from the data, given by

$$\hat{G}(i\omega) \;=\; \frac{Y(i\omega)}{U(i\omega)}, \tag{6}$$

where $Y(i\omega)$ and $U(i\omega)$ are the discrete Fourier transform of the output and input timeseries. The Bode plots of the ETFEs for 60, 65, and 70 slpm are shown in Fig. 8, where the errorbars correspond to one standard deviation from the mean. The responses roll off above in the 700–800 Hz range, which is consistent with the dynamics of jets with similar velocities identified in [19]. The flow rate considered is 65 slpm herein.

A transfer function was fitted to the frequency response data at 65 slpm using MATLAB's System Identification

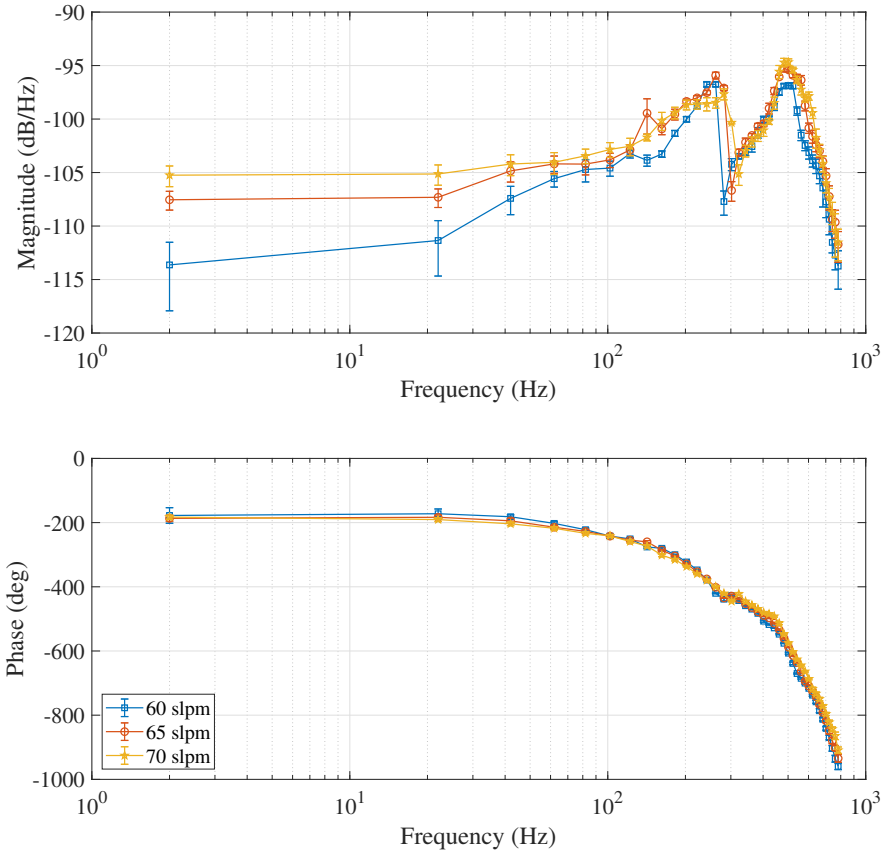

Fig. 8 Experimentally-determined frequency responses (ETFEs) at several flow rates.

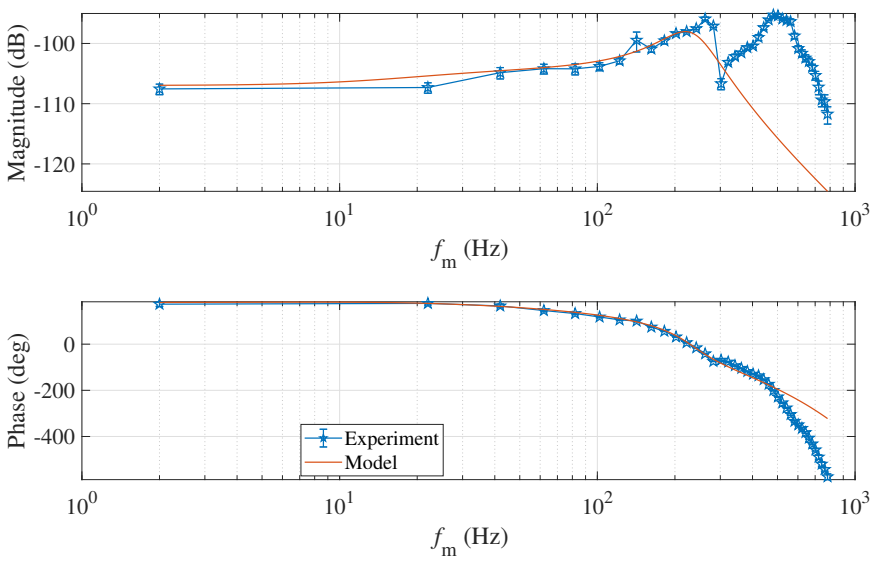

Fig. 9 Frequency response: transfer function model fit to experimental data.

Toolbox. While all the features could be captured with an 8-pole, 7-zero model, the closed-loop dynamics are shown in section VI to be limited by factors other than open-loop bandwidth, so that only the first resonance in Fig. 8 needs to be captured by model. Consequently, a simpler 3-pole, 1-zero transfer function model was used for control design, given by

$$G(s) = e^{-1.2\times10^{-3}s}\,\frac{-13.2(s+102)}{(s+139)(s^2+735s+2.16\times10^6)} \tag{7}$$

The frequency response of (7) is shown along with the experimental data in Fig. 9. The system delay is a result of the transport time of particles acted on by the piezo at the nozzle orifice to travel to the pitot probe in the outlet channel, a distance of around 50 mm. This corresponds to a transport velocity of approximately 42 m/s, while the mean nozzle velocity is around 100 m/s. The ratio of transport velocity to mean nozzle velocity is in the vicinity of that found in a similar fluidic device in [19].

VI. Controller design

The objective in this paper is to produce a variable frequency oscillation that can track a reference sinusoidal signal. Consequently, we adopted a phased-locked loop (PLL) controller architecture, for which the standard form is shown in Fig. 10. The signal generated by the voltage-controlled oscillator (VCO) is compared with the measured or reference signal to produce an error signal related to their phase difference. The error signal is filtered and used as a proportional feedback signal to adjust the VCO frequency. The architecture for the PLL in the present work is shown in Fig. 11; Fig. 11a shows the nonlinear implementation of the system, while Fig. 11b shows the linearised representation that was

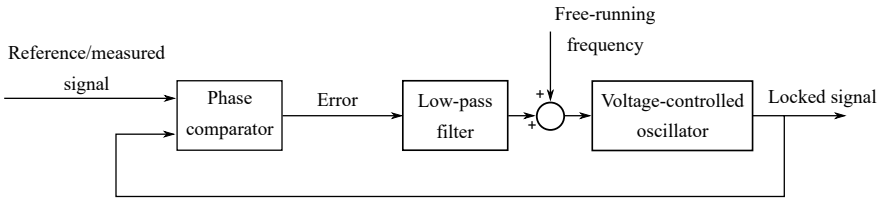

Fig. 10 Standard phase-locked loop (PLL) architecture

used for analysis and control design. The standard linearisation assumption has been made for the (left-hand side) mixer [41], such that the output goes from the cosine oscillation signal to the phase signal, $\phi_y(t)$. In the linearised system, the only signal time scale (or frequency) is that of $u(t)$, i.e. the signal that modulates the 2.5 kHz piezo tone amplitude. This is because the nonlinear operators in Fig. 11a between $u(t)$ and the output of the mixer (on the left) can be replaced the equivalent components of the linear system in Fig. 11b. This can be explained by considering the operations performed, whose effect on the spectrum of each signal is sketched in Fig. 12.

1) The input, $u(t)$, is at baseband before being amplitude-modulated onto the carrier signal in the FPGA.
2) The resulting AM excitation signal is demodulated by the jet dynamics to baseband [42–44], and is then modulated onto the frequency of the oscillation by the fluidic oscillator.
3) The mixer demodulates the resulting FM signal that is measured by the pitot probe, producing an error signal at baseband, i.e. at the time scale of $u(t)$, and a sum frequency.
4) The lower-pass filter attenuates the sum frequency term.

In this system, the fluidic oscillator serves the purpose of the VCO, the free-running frequency is $f_{\text{osc, nat}}$, the input to the VCO is the amplitude of the 2.5 kHz excitation tone applied to the piezo amplifier, and the reference signal is the desired output trajectory for the oscillator. In addition to the proportional feedback used in the standard architecture, an integral term, K_I/s, is included. Without an integral term, the PLL achieves frequency lock but not phase lock, since a non-zero error signal is required to drive the required steady input amplitude. The natural oscillation frequency, $f_{\text{osc, nat}}(t)$, was assumed constant up to this point. However, a time-dependence is now included to indicate that its value wanders, which constitutes an output disturbance.

The mixer output is

$$D(t)\cos\left(2\pi f_{\text{osc}}(t)\right)\,\sin\left(2\pi f_{\text{ref}}\right) \;=\; \frac{D(t)}{2}\left[\sin\left(2\pi\left(f_{\text{ref}}-f_{\text{osc}}(t)\right)\right)+\sin\left(2\pi\left(f_{\text{ref}}+f_{\text{osc}}(t)\right)\right)\right], \tag{8}$$

where f_{ref} is the reference frequency. The difference frequency can be written as

$$\frac{D(t)}{2}\sin\left(2\pi\left(f_{\text{ref}}-f_{\text{osc}}(t)\right)\right) \;=\; \frac{D(t)}{2}\sin\left(\phi_r(t)-\phi_y(t)\right) \;\approx\; \frac{D(t)}{2}\left(\phi_r(t)-\phi_y(t)\right), \tag{9}$$

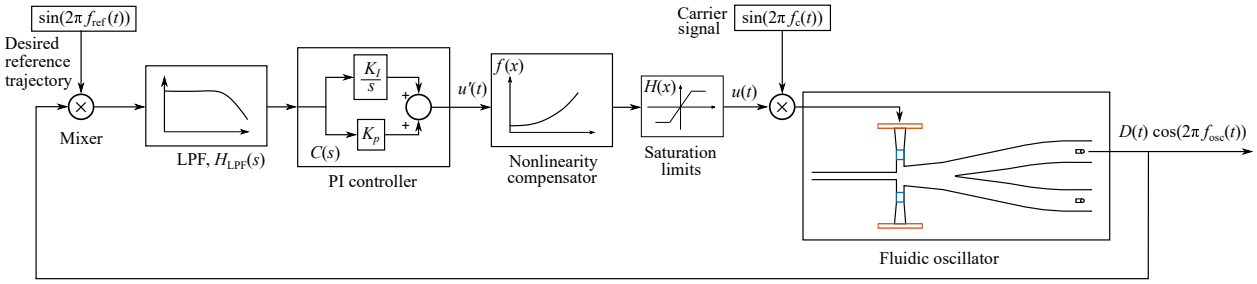

(a) Nonlinear implementation

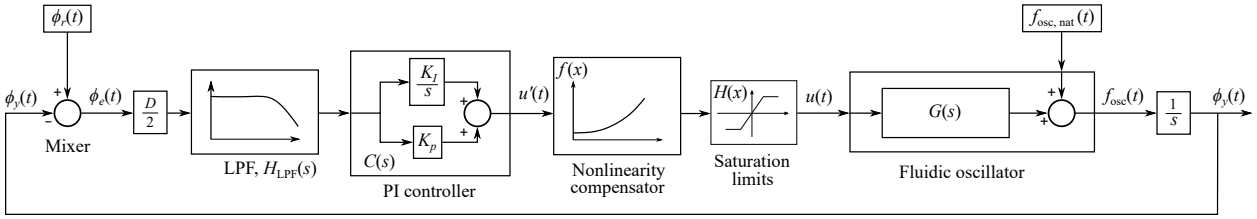

(b) Linearised representation

Fig. 11 Phase-locked loop architecture in present work

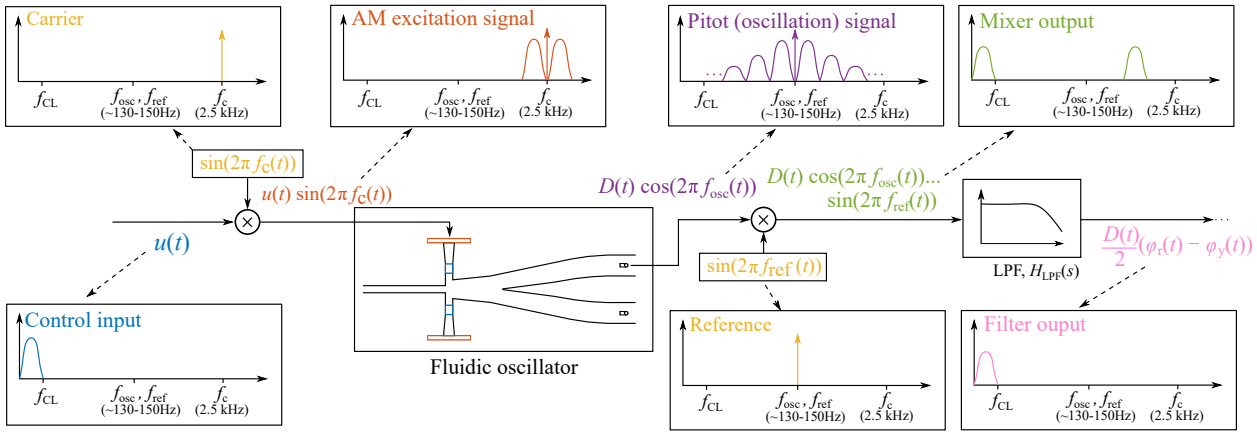

Fig. 12 Sketches of spectra of signals between control input and low-pass filter output.

where $\phi_r(t)$ and $\phi_y(t)$ are the phases of the reference and oscillation signals, respectively. Note that the factor of $D/2$ in Fig. 11b reflects the same factor in (9), which is an outcome of the mixer. The dependence of D on time in (9) is removed by the nonlinearity compensator, as discussed below.

Without removal, the sum frequency term in (8) would cause a perturbation in the oscillation phase at $f_{\text{ref}} + f_{\text{osc}}(t) \approx 2f_{\text{osc}}(t)$, which is between 260 and 300 Hz at 65 slpm. In addition, the sum frequency signal causes the control input to saturate routinely, introducing unmodelled nonlinearity and significantly degrading the controller performance. The low-pass filter is used to remove the sum frequency term in (8).

Saturation limits keep the input voltage in the range $0 \leq u \leq 0.93\,\text{V}_{\text{RMS}}$ to avoid damaging the piezo buzzer. The combination of saturation limits and an integral term in the controller would typically require a scheme to avoid integrator windup. An anti-windup strategy is not necessary in this case because the error signal is a phase and is therefore limited to the range $-\pi \leq \phi_e(t) \leq \pi$. If the reference frequency is outside the envelope of the controller, the error will cycle through this range at a rate equal to the difference between the output and reference frequencies, and the integrator will not wind up.

The nonlinearity compensator is a gain that accounts for the effect of the oscillation amplitude, $D(t)$, decreasing with respect to the excitation voltage (Fig. 6a). While it is the phase of the output that is relevant to the controller, the phase comparator is implemented with a mixer, so the amplitude of the oscillation is incorporated into the error signal ($D(t)$ in (8)). Without compensating for the amplitude of the oscillation, the error signal would be scaled down at larger input voltages, and the overall system gain would be reduced when the reference frequency is lower. This would make the controller less effective at either higher or lower reference frequencies, depending on the operating point for design. This is avoided through use of a compensating curve that scales the input voltage. Figure 13a shows the oscillation amplitude data on a linear scale (note that these are the same data as the 65 slpm curve in Fig. 6a) against input voltage, along with a fitted quadratic curve, and Fig. 13b shows the inverted curve that is implemented as a gain dependent on the input voltage. Such an inversion curve was used for each flow rate in the system identification experiments in section V.

The gain is denoted $f(x)$, and the saturation function is $H(x)$, such that the input that drives the piezo amplifier is given by

$$u(t) = H\left(f\left(u'(t)\right)u'(t)\right), \tag{10}$$

where u' is the pre-scaled input produced by the controller. With this implemented, the lower oscillation amplitude, $D(t)$, associated with larger values of $u(t)$ is cancelled out by the gain, $f(x)$. As such, the oscillation amplitude effectively

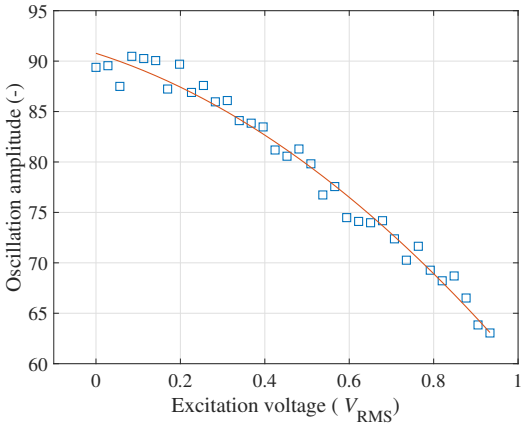

(a) Oscillation amplitude vs excitation voltage: experimental data (blue, squares), and fitted quadratic curve (red).

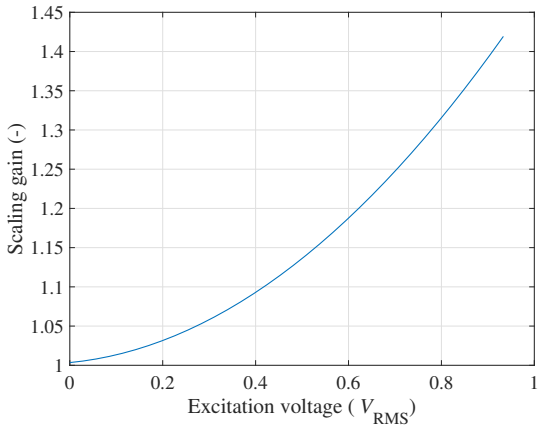

(b) Gain (nonlinearity compensator), $f(x)$

Fig. 13 Nonlinearity compensation

becomes a constant, D. The nonlinearity compensator and the linear approximation to the mixer make a linear analysis possible.

The controller parameters, K_I and K_p, along with the parameters of the low-pass filter, $H_\mathrm{LPF}(s)$, were determined by consideration of the closed-loop frequency response and the stability margins. Simulations were conducted that included either the true, nonlinear implementation of the mixer or its linear approximation in order to determine the degree of uncertainty introduced by the linearisation approach. The open- and closed-loop transfer functions are given by

$$L(s) = \frac{1}{2} D\, H_\mathrm{LPF}(s) C(s) G(s) \frac{1}{s} \qquad T(s) = \frac{L(s)}{1 + L(s)}, \tag{11}$$

where the factor of $1/2$ in $L(s)$ results from the operation of the mixer (see (8)). The closed-loop bandwidth was limited by the low-pass filter roll-off frequency, which must have rolled-off to a sufficient extent to attenuate the sum frequency at $f_\mathrm{ref} + f_\mathrm{osc}(t)$. A second-order filter was used because higher-order filters introduced greater phase lags that degraded the stability margins. The low-pass filter cut-off frequency was set to $f_\mathrm{LPF} = 50\,\mathrm{Hz}$ as a compromise between closed-loop bandwidth and attenuation of the sum term from the mixer. The period corresponding to this cut-off frequency is large compared with the delay in the system transfer function (11), so the delay could be ignored for control design purposes. The controller gains were then set to shape the closed-loop frequency response, while maintaining a phase margin of around 60^o and a gain margin of at least 6 dB. The closed-loop Bode plot is shown in Fig. 14. This response was achieved with the gains set to

$$K_\mathrm{I} = -15, \qquad K_\mathrm{p} = -5, \tag{12}$$

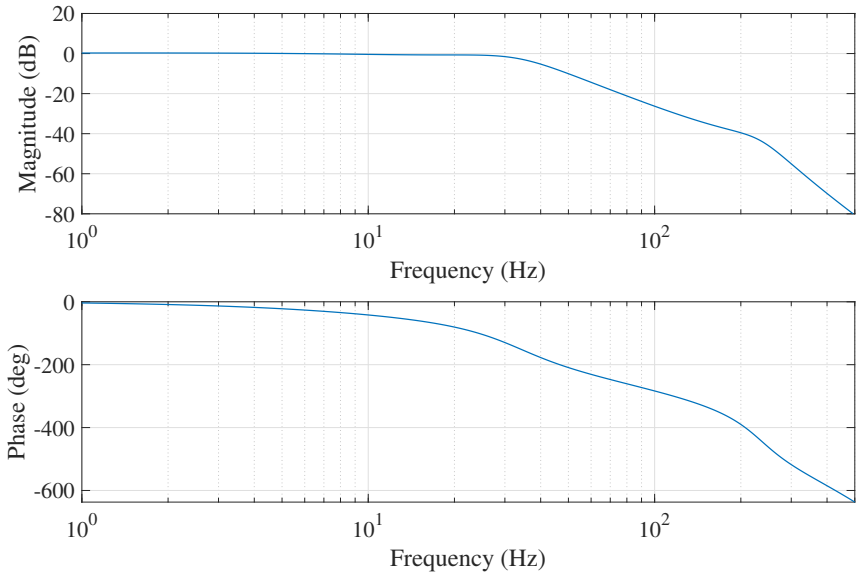

Fig. 14 Closed-loop bode plot

and the resulting gain and phase margins were 10.2 dB and 59.1°, respectively. The −3 dB frequency for the closed-loop magnitude response in Fig. 14 is 28 Hz, which would indicate an approximate response time of $1/28 = 36$ ms. Since the closed-loop bandwidth is limited by the low-pass filter, the decision to model the dynamics with a relatively simple transfer function is justified.

It is important to emphasize that the closed-loop bandwidth is that of closed-loop phase tracking function, rather than the output signal frequency. In other words, changes in the reference signal phase will be tracked with response time of 36 ms, but the reference signal frequency itself can be within the authority of actuation implied by the device characterisation in Fig. 5.

VII. Controller performance

The controller was tested first by setting the reference frequency to several values within the range of authority of the piezo. Figure 15 shows the reference signal and the oscillation signal as measured by the pitot probe, scaled and shifted to have the same RMS and mean as the reference signal. Figures 15a, 15b, and 15c show cases where the reference frequency is comfortably within the lock range of the controller ($f_{\text{ref}} = 145,\ 140,$ and 135 Hz). Figure 15d is a limiting case on the boundary of the lock range ($f_{\text{ref}} = 130$ Hz), and shows that the controller has diminished authority to reject disturbances to the phase whilst simultaneously holding the oscillation frequency at the reference value. The disturbances to the phase stem from random fluctuations in entrainment that affect the feedback mechanism as well as variations in mass flow rate. These figures demonstrate the controller's effectiveness at rejecting disturbances and

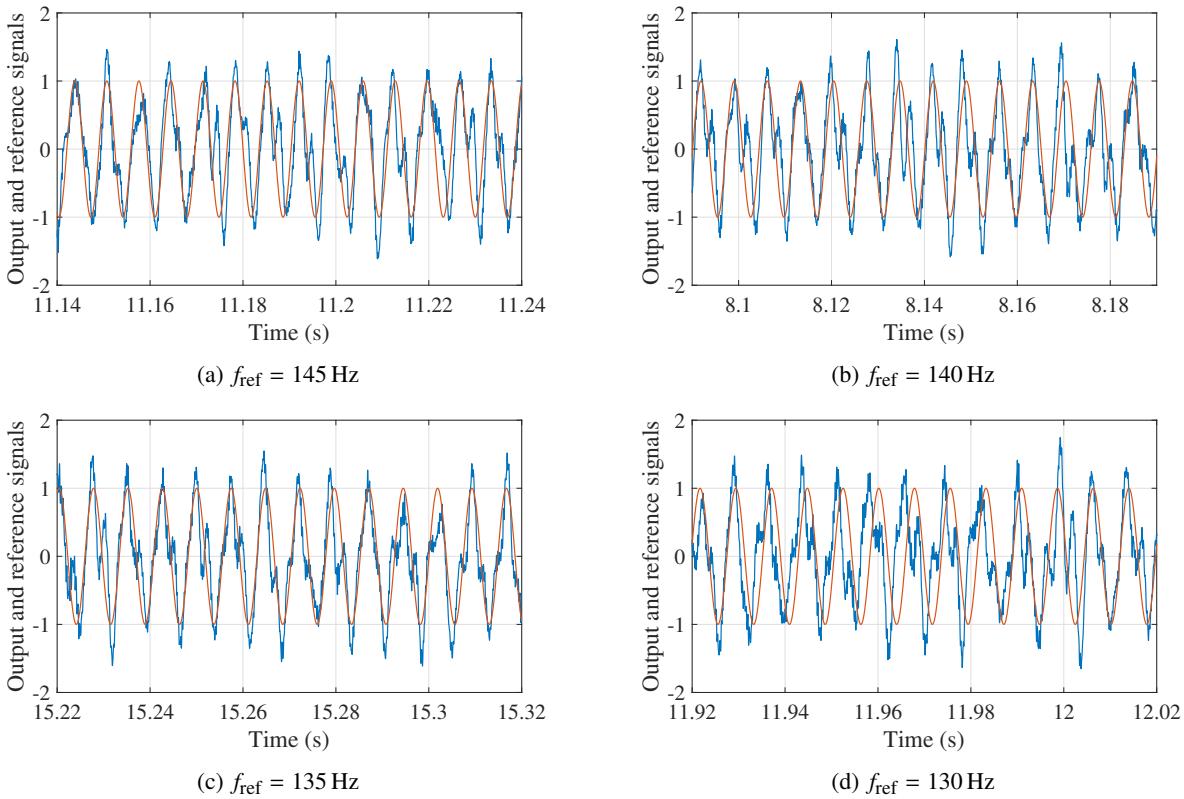

(a) $f_{\text{ref}} = 145\,\text{Hz}$ (b) $f_{\text{ref}} = 140\,\text{Hz}$

(c) $f_{\text{ref}} = 135\,\text{Hz}$ (d) $f_{\text{ref}} = 130\,\text{Hz}$

Fig. 15 Closed-loop controller at several reference signal frequencies: scaled pitot measurement (blue) and reference signal (red) vs time.

maintaining the phase lock. The lock-range of the controller is effectively the region between the unexcited and excited curves of oscillation frequency vs flow rate in Fig. 5.

The effect of the controller is illustrated by the spectrum of the oscillation signal. Figure 16 shows the power spectral density of time series measurements of the oscillation signal without excitation, with a constant (open-loop) excitation to give an oscillation frequency of $f_{\text{osc}} \approx 140\,\text{Hz}$, and with the closed-loop controller operating with the reference frequency set to $f_{\text{ref}} = 140\,\text{Hz}$. These are effectively two-sided phase noise plots [45, p. 15]. The unexcited data show a broad peak centred on ~149 Hz. The spread of power across a relatively wide range of frequencies indicates a relatively large phase noise of the oscillation, caused by disturbances to the oscillation frequency and phase that cause the phase to wander from a purely harmonic signal at a constant frequency. For example, the mass flow controller produces small variations in flow rate, which translate to a varying oscillation frequency. The effect of the constant excitation is to shift the centre of the broad peak to a lower frequency, as shown by the red curve in Fig. 16. When the controller is used, the power across the broad peak is concentrated into a small number of frequency bins, indicating that the phase noise is significantly reduced—the wandering phase has been eliminated. This demonstrates that the bandwidth of disturbances causing the variation in phase and frequency is within the closed-loop bandwidth of the

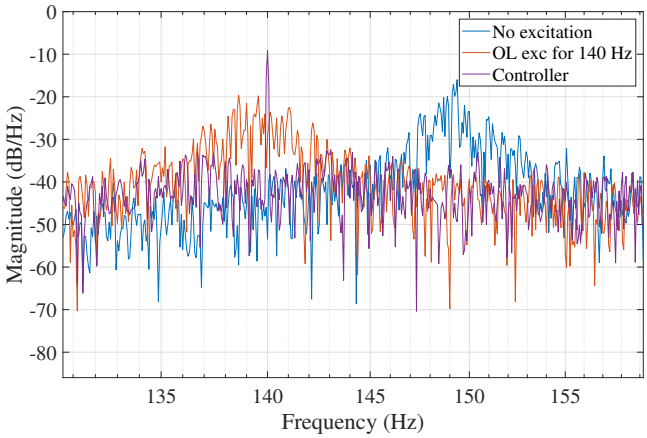

Fig. 16 Power spectral density: unexcited (blue), open-loop excitation to give $f_{\text{osc}} \approx 140\,\text{Hz}$ (red), and closed-loop controller with $f_{\text{ref}} = 140\,\text{Hz}$ (purple).

controller.

The controller was also tested by introducing a step change in the reference signal phase. Forty step response experiments were conducted with a phase step of 90° at $t = 1\,\text{s}$, so that ensemble averaging could be used to extract the mean response and the mean control signal. Figure 17 shows the oscillation and reference signals as well as the control input. The closed-loop response time was predicted to be around 36 ms in section VI, which is well matched by the experimental closed-loop response in the figure. If the control signal is used to calculate the response time, then the time the control signal is above the threshold of 10% of the difference between its steady state and peak values is 35.5 ms.

Figure 18 shows the results of an experiment where the request to the mass flow controller was step-changed in order to demonstrate the benefit of the closed-loop controller. First, open-loop control was used by setting the excitation voltage to the value that gives approximately 138 Hz at 65 slpm according to Fig. 6b. At $t = 10\,\text{s}$, the mass flow rate request was changed to 62 slpm. To illustrate the ineffectiveness of this approach, we have calculated the hypothetical error signal that would be generated by the closed loop controller given the pitot signal during this open-loop experiment and a reference oscillation at the target frequency. This error signal is given by $e(t) = \mathcal{L}^{-1}\left\{H_{\text{LPF}}(s)Y_{\text{mix}}(s)\right\}$, where $Y_{\text{mix}}(s)$ is the Laplace transform of the mixer output. This signal is shown in Fig. 18b, the mass flow rates requested and achieved by the mass flow controller are shown in Fig. 18a, and the control input voltage in Fig. 18d. An arbitrary 150 ms section of the raw pitot data during the step is shown in Fig. 18c alongside the reference signal.

The error signal in Fig. 18b cycles through a phase range of π to $-\pi$, scaled by oscillation amplitude, at a rate equal to the error in the oscillation frequency, given by $f_{\text{ref}} - f_{\text{osc}}$. Before the change in mass flow rate, the frequency

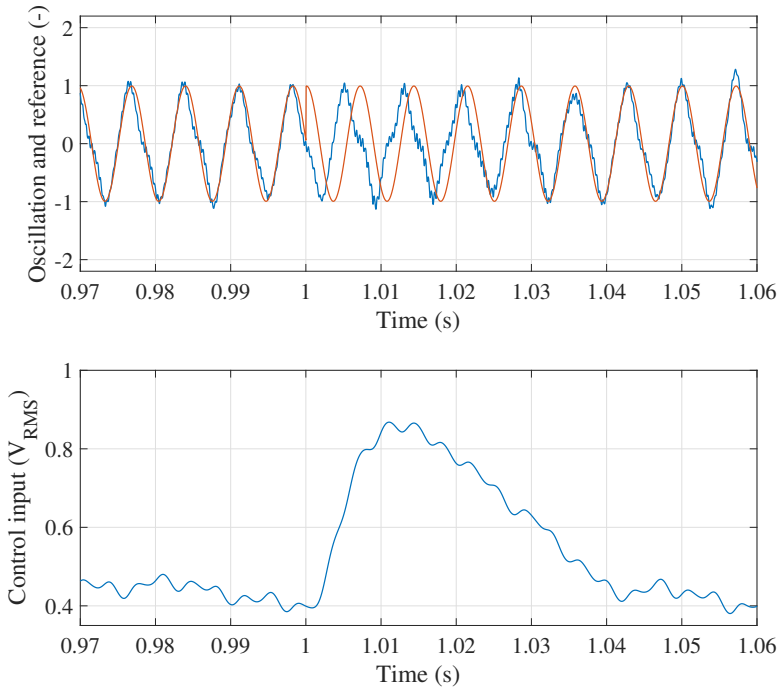

Fig. 17 Ensemble averaged step response (n = 40) to 90^{o} reference phase step: oscillation (blue) and reference (red) signals (top) and control input (bottom).

error is small because the open-loop excitation voltage was chosen to match (approximately) the reference frequency. As such, the period of the error signal is small. However, as the mass flow rate drops and the oscillation frequency reduces, the frequency error increases, which is reflected by the error signal cycling through the full (scaled) phase range more quickly. This can be observed in the section of the pitot and reference signals in Fig. 18c, which shows that the oscillator initially leads the reference, then lags increasingly throughout the section until it is close to being in anti-phase by the end.

This experiment was repeated using closed-loop control. The error signal, the requested and achieved mass flow rates, the control input signal, and the equivalent 150 ms section of the pitot and reference signals, are shown in Fig. 19. The response time of the mass flow controller is evidently larger than that of the closed-loop controller, which is able to maintain phase-lock throughout. In the closed-loop case, the controller error is a phase noise signal rather than the periodic signal observed in the open-loop case (Fig. 18b), which signifies an error in frequency.

VIII. Summary and conclusions

Piezoelectric buzzers were added to a fluidic oscillator of the type first studied by Spyropoulos [22] (one feedback tube) in order to modify the feedback mechanism and influence the oscillation frequency. The device was characterised statically by measuring the oscillation frequency with respect to flow rate both with and without acoustic excitation from

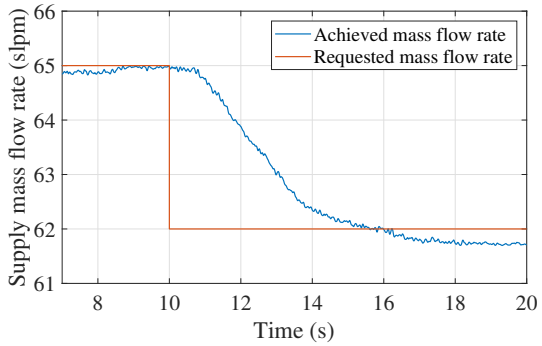

(a) Mass flow rate signal: requested (red) and achieved (blue).

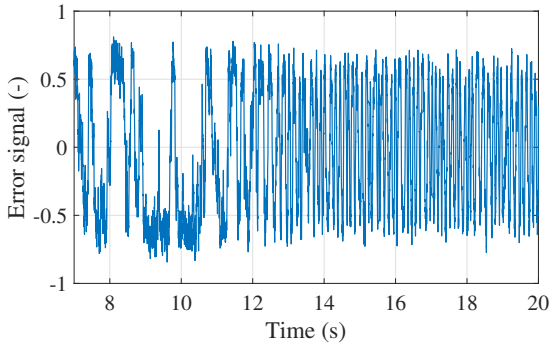

(b) Hypothetical controller error signal.

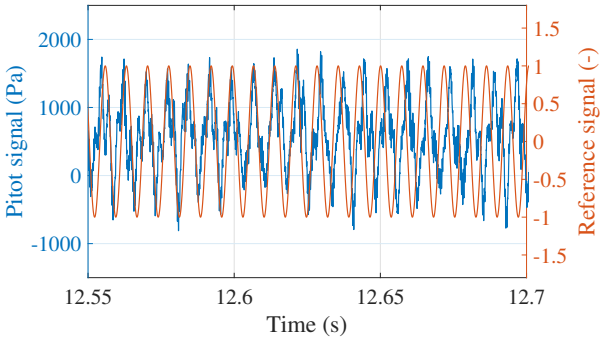

(c) Pitot signal (blue) and reference signal (red), zoomed view.

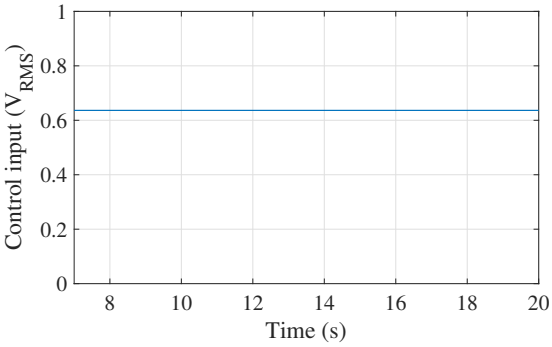

(d) Control input signal.

Fig. 18 Mass flow rate disturbance: open-loop controller response.

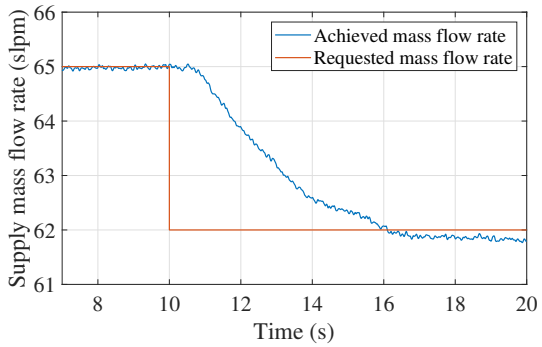

(a) Mass flow rate signal: requested (red) and achieved (blue).

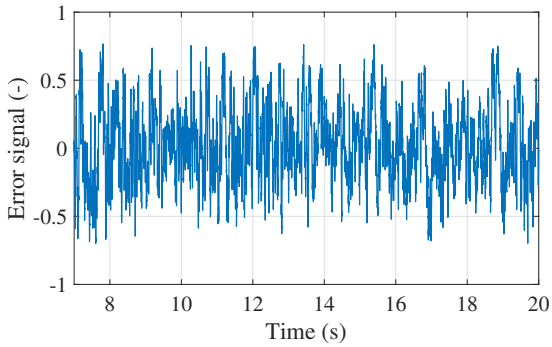

(b) Controller error signal.

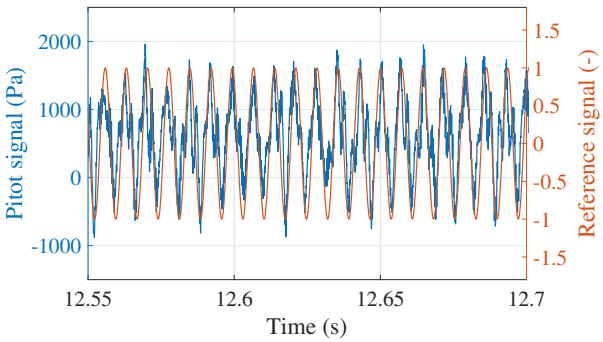

(c) Pitot signal (blue) and reference signal (red), zoomed view.

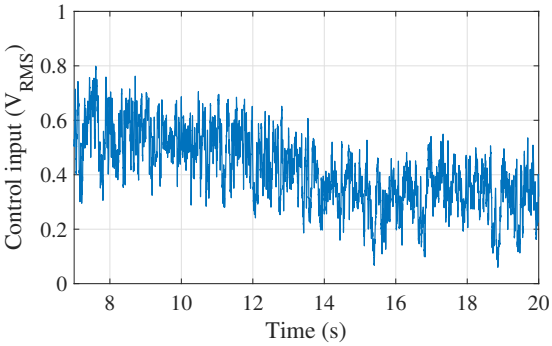

(d) Control input signal.

Fig. 19 Mass flow rate disturbance: closed-loop controller response.

one of the piezos. The effect of excitation was shown to be a reduction in the oscillation frequency at the majority of flow rates. At a fixed flow rate, the oscillation frequency and magnitude were shown to reduce linearly with respect to excitation amplitude. It was explained that the device operates as an AM-FM converter, because a modulating signal applied to the amplitude of the acoustic excitation is demodulated by the jet, then remodulated onto the oscillation frequency. The system output was taken as the change in oscillation frequency resulting from the excitation, and the system input was the modulation signal applied to the excitation amplitude. System identification experiments were conducted at several flow rates where the modulation signal was set to be a sinusoid with a frequency that was stepped through a series of test values. The pitot signal was recorded and a frequency discriminator was applied in order to demodulate the data and produce the output signal. The magnitude and phase of the output were calculated, and a transfer function model was fitted to the 65 slpm case.

A phase-locked loop controller structure was adopted, where the voltage-controlled oscillator was replaced with the piezo-fluidic oscillator, and a PI controller was used instead of the traditional proportional feedback. A nonlinearity compensator was implemented to remove the effect of the oscillation magnitude decreasing with respect to excitation voltage, which was otherwise incorporated into the phase error signal. The low-pass filter in the PLL was required to eliminate the sum frequency present in the mixer output. This filter limited the closed-loop bandwidth, but was necessary to prevent the sum frequency appearing in the control input and causing it to saturate. The proportional and integrator gains were set by tuning the shape of the closed-loop frequency response while maintaining acceptable stability margins. The controller was implemented experimentally, and tests were conducted to assess its performance at driving the oscillation phase to that of a reference sinusoid. The disturbances that cause the frequency and phase to wander were rejected when the controller was switched on, and the oscillation phase was locked to the reference phase. Another experiment involved a step change in the reference signal phase, which was repeated to allow the oscillation signal and control input to be ensemble averaged. This tested the dynamic response of the controller to the reference signal, and indicated that the closed-loop response time matched closely the predicted value from the theory and model. Experiments were conducted where the mass flow rate request was step-changed by approximately -5% and the performance of the closed-loop controller was compared with the open-loop case. In the open-loop case, the excitation voltage was set to the value that would result in approximately the target oscillation frequency at the initial mass flow rate. However, even when the mass flow rate is known, phase-lock could not be achieved without feedback. When the mass flow rate changed, the measured oscillation frequency deviated further from the target frequency. In the closed-loop case, the controller was able to maintain phase-lock throughout.

The first conclusion of this paper is that it is possible to influence the oscillation frequency of a sonic oscillator using acoustic excitation. Once the working mechanism is better understood, refinement of the device design is likely to

yield an improvement in the acoustic authority over the oscillation frequency. The second conclusion is that feedback information from a practical measurement can be used to achieve a closed-loop bandwidth (with respect to disturbances to the oscillation phase) equal to 20% of the oscillation frequency, which was sufficient to reject all disturbances that would otherwise cause the phase to wander. The robustness of the controller to variations in the supply mass flow rate is aided by the competing effects of changing oscillation magnitude (increases with respect to flow rate) and piezo authority (reduces with respect to flow rate) on the system DC gain. This robustness could be improved by decoupling the oscillation magnitude from the error signal. This could be achieved by implementing another phase-locked loop to track the oscillation signal, producing a unity-amplitude sinusoid whose phase could be subtracted directly from the reference phase. This modification would result in an improved robustness to mass flow rate variations at the expense of closed-loop bandwidth, since the additional phase-locked loop would introduce a time constant. We note that the limiting factor for the closed-loop bandwidth was the cut-off frequency of the low-pass filter that is used to attenuate the sum frequency from the mixer output. The required filter cut-off frequency scales with the oscillation frequency, hence the closed-loop bandwidth should also scale with the oscillation frequency. This predicted scaling holds promise for applications where higher oscillation frequencies are required.

Appendix

It is assumed here that the pitot signal, p_{out}, is measured during experiments where the amplitude modulation signal given by (2) is applied to the piezo amplifier. The frequency discrimination method applied to the pitot data consists of a derivative with respect to time, follow by a modulus operation, given by

$$z = \left| \frac{\mathrm{d}p_{\text{out}}}{\mathrm{d}t} \right|. \tag{13}$$

Substituting the expression for p_{out} from (3) into (13), and assuming a constant oscillation amplitude, D, gives

$$z = 2\pi D \left(f_{\text{osc,exc}} + k_{\text{f}} \sin\left(2\pi f_{\text{m}} t + \phi\right) \right) \left| \cos\left(2\pi \left[f_{\text{osc,ex}} t + k_{\text{f}} \int_{\tau=0}^{\tau=t} \sin\left(2\pi f_{\text{m}} \tau + \phi\right) \mathrm{d}\tau \right] \right) \right|. \tag{14}$$

where the modulus operation can be applied to the cosine only because the term multiplying the cosine is always positive. The rectified cosine can be replaced with its Fourier series, giving

$$z = 2\pi D \left(f_{\text{osc,exc}} + k_{\text{f}} \sin\left(2\pi f_{\text{m}} t + \phi\right) \right) \left(\frac{2}{\pi} + \frac{4}{\pi} \sum_{n=1}^{n=\infty} \frac{(-1)^n}{1-4n^2} \cos\left(2\pi \left[2n f_{\text{osc,ex}} t + 2nk_{\text{f}} \int_{\tau=0}^{\tau=t} \sin\left(2\pi f_{\text{m}} \tau + \phi\right) \mathrm{d}\tau \right] \right) \right). \tag{15}$$

The spectral content of the terms in (15) was analysed numerically in MATLAB for several values of f_{m} relative to $f_{\text{osc,exc}}$. The constant component of the Fourier series multiplies the term in $\sin\left(2\pi f_{\text{m}} t + \phi\right)$, giving a response at f_{m}.

The remaining products give an FM spectrum around the even harmonics of $f_{\mathrm{osc,exc}}$, with modulation frequency f_{m}. The signal power at f_{m} was shown to be independent of the terms of the Fourier series apart from the constant term, with the exception of when f_{m} was equal to f_{osc} or its even harmonics. This demonstrates that the signal with spectral content at f_{m} in the output of the frequency discriminator is given by

$$z_{f_{\mathrm{m}}} = 4Dk_{\mathrm{f}} \sin\left(2\pi f_{\mathrm{m}} t + \phi\right). \tag{16}$$

The magnitude and phase of the transfer function, $\hat{G}(i2\pi f_{\mathrm{m}})$, can therefore be found by calculation of the magnitude and phase of the demodulated pitot signal at the frequency bin corresponding to f_{m}. The expression (16) shows that phase-coherent averaging is possible because the phase of the signal is determined by the input phase, $f_{\mathrm{m}}t$, and the combination of the transport delay and the transfer function phase response, ϕ.

Acknowledgements

The authors gratefully acknowledge the support of this work by Rolls-Royce and the EPSRC program grant (EP/P000878/1).

References

[1] Aram, S., and Shan, H., "Synchronization effect of an array of sweeping jets on a separated flow over a wall-mounted hump," *AIAA Aviation 2019 Forum*, 2019, p. 3396.

[2] Buzica, A., Bartasevicius, J., and Breitsamter, C., "Experimental investigation of high-incidence delta-wing flow control," *Experiments in Fluids*, Vol. 58, No. 9, 2017, p. 131.

[3] Cattafesta III, L. N., and Sheplak, M., "Actuators for active flow control," *Annual Review of Fluid Mechanics*, Vol. 43, 2011, pp. 247–272.

[4] Culley, D. E., Bright, M. M., Prahst, P. S., and Strazisar, A. J., "Active flow separation control of a stator vane using embedded injection in a multistage compressor experiment," *Journal of Turbomachinery*, Vol. 126, No. 1, 2004, pp. 24–34.

[5] Steinfurth, B., Haucke, F., and Weiss, J., "Assessment of two fluidic actuators for active flow control on a one-sided diffuser," *CEAS Aeronautical Journal*, Vol. 10, No. 2, 2019, pp. 633–643.

[6] Staats, M., Löffler, S., Ebert, C., Grund, T., and Weiss, J., "A Fluidic Device for Active Flow Control: Simulation vs. Experiment with Emphasis on Application," *2018 Applied Aerodynamics Conference*, 2018, p. 3336.

[7] Bauer, M., Lohse, J., Haucke, F., and Nitsche, W., "High-lift performance investigation of a two-element configuration with a two-stage actuator system," *AIAA Journal*, Vol. 52, No. 6, 2014, pp. 1307–1313.

[8] Whalen, E. A., Shmilovich, A., Spoor, M., Tran, J., Vijgen, P., Lin, J. C., and Andino, M., "Flight test of an active flow control enhanced vertical tail," *AIAA Journal*, Vol. 56, No. 9, 2018, pp. 3393–3398.

[9] Raman, G., and Raghu, S., "Cavity resonance suppression using miniature fluidic oscillators," *AIAA Journal*, Vol. 42, No. 12, 2004, pp. 2608–2612.

[10] Bae, J., Breuer, K. S., and Tan, C. S., "Active control of tip clearance flow in axial compressors," *ASME Turbo Expo 2003, collocated with the 2003 International Joint Power Generation Conference*, American Society of Mechanical Engineers, 2003, pp. 531–542.

[11] Auld, A., Hilfer, M., Hogg, S., Ingram, G., and Messenger, A., "Application of an air-curtain fluidic jet type seal to reduce turbine shroud leakage," *ASME Turbo Expo 2013: Turbine Technical Conference and Exposition*, American Society of Mechanical Engineers, 2013, pp. V03AT15A005–V03AT15A005.

[12] Tang, B. M., Bacic, M., and Ireland, P. T., "Effect of Active Modulation of Through-Casing Coolant Injection on Turbine Efficiency," *ASME Turbo Expo 2017: Turbomachinery Technical Conference and Exposition*, American Society of Mechanical Engineers, 2017, p. V02AT40A031.

[13] Raman, G., Packiarajan, S., Papadopoulos, G., Weissman, C., and Raghu, S., "Jet thrust vectoring using a miniature fluidic oscillator," *The Aeronautical Journal (1968)*, Vol. 109, No. 1093, 2005, p. 129–138. doi:10.1017/S0001924000000634.

[14] Jahanmiri, M., "Active flow control: a review," Tech. rep., Chalmers University of Technology, 2010.

[15] Gregory, J. W., Gnanamanickam, E. P., Sullivan, J. P., and Raghu, S., "Variable-frequency fluidic oscillator driven by a piezoelectric bender," *AIAA Journal*, Vol. 47, No. 11, 2009, pp. 2717–2725.

[16] Mair, M., Chen, L.-W., Turner, J., Bacic, M., and Ireland, P., "Experimental and Numerical Analysis of a Piezo Driven Fluidic Device for Active Flow Control," *52nd AIAA/SAE/ASEE Joint Propulsion Conference*, 2016, p. 4860.

[17] Mair, M., Bacic, M., and Ireland, P., "On Dynamics of Acoustically Driven Bistable Fluidic Valves," *J. Fluids Engng*, Vol. 141, No. 6, 2019, p. 061202.

[18] Mair, M., and Bacic, M., "Fluid Dynamics of a Bistable Diverter Under Ultrasonic Excitation—Part I: Performance Characteristic," *J. Fluids Engng*, Vol. 143, No. 7, 2021, p. 071201.

[19] Nicholls, C. J., and Bacic, M., "Closed-Loop Control of a Piezo-Fluidic Amplifier," *AIAA Journal*, Vol. 58, No. 6, 2020, pp. 2414–2427. doi:10.2514/1.J059305, URL `https://doi.org/10.2514/1.J059305`.

[20] Gregory, J., and Tomac, M. N., "A review of fluidic oscillator development," *43rd AIAA Fluid Dynamics Conference*, 2013, p. 2474.

[21] Warren, R. W., "Negative feedback oscillator," , Nov. 24 1964. US Patent 3,158,166.

[22] Spyropoulos, C. E., "A Sonic Oscillator," *Proceedings of the Fluid Amplification Symposium*, Vol. III, Washington D.C., 1964, pp. 27–51.

[23] Sundström, E. T., and Tomac, M. N., "Aeroacoustic Characteristics of a Synchronized Fluidic Oscillator," *Flow, Turbulence and Combustion*, Vol. 106, No. 1, 2021, pp. 61–77.

[24] Gokoglu, S., Kuczmarski, M., Culley, D., and Raghu, S., "Numerical studies of a fluidic diverter for flow control," *39th AIAA Fluid Dynamics Conference*, 2009, p. 4012.

[25] Coandă, H., "Device for deflecting a stream of elastic fluid projected into an elastic fluid," , Sep. 1 1936. US Patent 2,052,869.

[26] Tomac, M. N., and Sundström, E. T., "Adjustable frequency fluidic oscillator with supermode frequency," *AIAA Journal*, Vol. 57, No. 8, 2019, pp. 3349–3359.

[27] Sundström, E. T., and Tomac, M. N., "Synchronization and flow characteristics of the opposed facing oscillator pair in back-to-back configuration," *Flow, Turbulence and Combustion*, Vol. 104, No. 1, 2020, pp. 71–87.

[28] Gharib, M., "Response of the cavity shear layer oscillations to external forcing," *AIAA journal*, Vol. 25, No. 1, 1987, pp. 43–47.

[29] Stalnov, O., Fono, I., and Seifert, A., "Closed-loop bluff-body wake stabilization via fluidic excitation," *Theoretical and Computational Fluid Dynamics*, Vol. 25, No. 1, 2011, pp. 209–219.

[30] Nicholls, C. J., Tang, B. M. T., Turner, J., and Bacic, M., "Novel operating mode of a fluidic oscillator," *Journal of Fluids Engineering*, Vol. 144, No. 7, 2022, p. 071501. doi:10.1115/1.4053554, URL `https://doi.org/10.1115/1.4053554`.

[31] Bartlett, M. S., "Smoothing periodograms from time-series with continuous spectra," *Nature*, Vol. 161, No. 4096, 1948, pp. 686–687.

[32] Welch, P., "The use of fast Fourier transform for the estimation of power spectra: a method based on time averaging over short, modified periodograms," *IEEE Transactions on audio and electroacoustics*, Vol. 15, No. 2, 1967, pp. 70–73.

[33] Tesař, V., Hung, C.-H., and Zimmerman, W. B., "No-moving-part hybrid-synthetic jet actuator," *Sensors and Actuators A: Physical*, Vol. 125, No. 2, 2006, pp. 159–169.

[34] Lush, P. A., "Investigation of the switching mechanism in a large scale model of a turbulent reattachment amplifier," *2nd Cranfield Fluidics Conference, Cambridge, UK*, 1967.

[35] Lush, P. A., "A theoretical and experimental investigation of the switching mechanism in a wall attachment fluid amplifier," *IFAC Symposium on Fluidics*, 1968.

[36] Epstein, M., "Theoretical investigation of the switching mechanism in a bistable wall attachment fluid amplifier," *J. Basic Engng*, Vol. 93, No. 1, 1971, pp. 55–62.

[37] Crow, S. C., and Champagne, F. H., "Orderly structure in jet turbulence," *J. Fluid Mech.*, Vol. 48, No. 3, 1971, pp. 547–591.

[38] Wiltse, J. M., and Glezer, A., "Manipulation of free shear flows using piezoelectric actuators," *J. Fluid Mech.*, Vol. 249, 1993, pp. 261–285.

[39] Rapoport, D., Fono, I., Cohen, K., and Seifert, A., "Closed-loop vectoring control of a turbulent jet using periodic excitation," *Journal of Propulsion and Power*, Vol. 19, No. 4, 2003, pp. 646–654.

[40] Lathi, B. P., and Zhi, D., *Modern digital and analog communication systems*, Oxford University Press, Inc., 1995.

[41] Gupta, S., "Phase-locked loops," *Proceedings of the IEEE*, Vol. 63, No. 2, 1975, pp. 291–306. doi:10.1109/PROC.1975.9735.

[42] Glezer, A., and Amitay, M., "Synthetic jets," *Annual Review of Fluid Mechanics*, Vol. 34, No. 1, 2002, pp. 503–529.

[43] Nicholls, C. J., Chakravarthy, K., Tang, B. M. T., Williams, B. A. O., and Bacic, M., "On acoustically modulated jet shear layers and the Nyquist–Shannon sampling theorem," *Physics of Fluids*, Vol. 34, No. 11, 2022, p. 115106. doi:10.1063/5.0118025, URL `https://doi.org/10.1063/5.0118025`.

[44] Nicholls, C. J., Chakravarthy, K., Tang, B. M. T., Williams, B., and Bacic, M., "Shear layer response to overmodulated acoustic perturbations," *Physics of Fluids*, (in press) 2022. doi:10.1063/5.0130336, URL `https://doi.org/10.1063/5.0130336`.

[45] Rubiola, E., *Phase noise and frequency stability in oscillators*, Cambridge University Press, 2008.